Applied Surface Science 289 (2014) 502–510

Contents lists available at ScienceDirect

Applied Surface Science

journal homepage: www.elsevier.com/locate/apsusc

DFT study of benzene and CO co-adsorption on PtCo(1 1 1)

V. Orazi[b], J.S. Ardenghi[a,b], P. Bechthold[a,b], P.V. Jasen[a,b], M.E. Pronsato[a,b], E.A. González[a,b,*]

[a] Departamento de Física, Universidad Nacional del Sur, Av. Alem 1253, 8000 Bahía Blanca, Argentina
[b] IFISUR (UNS-CONICET), Av. Alem 1253, 8000 Bahía Blanca, Argentina

ARTICLE INFO

Article history:
Received 4 September 2013
Received in revised form 5 November 2013
Accepted 6 November 2013
Available online 19 November 2013

Keywords:
DFT
PtCo
Benzene
CO
Electronic structure

ABSTRACT

Co-adsorption of benzene and CO on PtCo(1 1 1) surface at low coverage is studied using density functional theory calculations. We investigated the PtCo FCT alloy surface with a uniform distribution. The most favorable site for CO is top on a Pt atom whereas for benzene is an HCP hollow site (formed by 2 Pt atoms and 1 Co atom). The co-adsorption energy is −1.62 eV. The calculations indicate a CO molecule with a ∼4° tilt angle with the normal to the surface. The most important bond is Pt—C_{CO}, as revealed by overlap population analysis. A very small CO–benzene interaction is also detected. The vibrational frequencies of adsorbed benzene and CO were also computed.

1. Introduction

Rising energy demands, depletion of fossil fuel reserves and environmental pollution has fueled the search for energy conversion devices with high efficiency and low emissions. Fuel cells powered by hydrogen or small organic molecules may have the potential to meet these requirements [1–3].

The catalytic conversion of aromatic molecules is a very important process in the chemical industry, both for environmental and economical reasons [4,5]. Hydrogenation or hydrogenolysis of these stable hydrocarbon molecules are the main target reactions in petroleum refining and reforming processes which are performed on transition metal catalysts. A strong incentive is provided by the European legislation, which has set a strict limit on the concentration of benzene and other aromatic molecules in fuels [6,7]. As a consequence, the bonding and coordination of aromatic compounds on transition metal surfaces continue to raise a large interest [8].

Benzene is a model compound for aromatic molecules, and although the chemisorption of this molecule has been studied from several experimental [9–12] and theoretical [4,5,13,14] approaches, the chemisorption or reactivity properties with respect to it remains an important issue to understand and optimize the catalytic performances.

Even if the basic aspects of benzene adsorption on transition metal surfaces are reasonably well understood, some important aspects are still the subjects of an active debate [8]. The possibility in some cases of obtaining multiple occupations of adsorption sites makes the picture even more complex.

First-principles calculations can bring additional and complementary insights to the problem. They especially provide information or analysis that cannot be easily extracted from experiments such as vibrational frequencies or intensities.

Besides the key electrocatalytic role they serve in fuel cells and glucose sensors, platinum-based catalysts are important components of automotive catalytic converters, CO gas sensors, petroleum refining, hydrogen production, and anticancer drugs. These applications uses platinum nanomaterials due to their catalytic ability to oxidize CO and NO_x, dehydrogenate hydrocarbons, and electrolyze water and their ability to inhibit the division of living cells [15].

Electrochemical gas sensors employing Pt catalysts have low power requirements, quick response, high stability, and linear output. The formation of oxygenated species at Pt sites on the electrode surface aids in the oxidation of CO to CO_2. While bulk Pt electrodes show modest CO oxidation characteristics at low concentrations, electrodes synthesized with Pt nano-materials show enhanced electrocatalytic activity toward CO oxidation. The development of electrochemical CO sensors with binary Pt-based nanostructured electrodes may help to increase sensitivity and decrease the

* Corresponding author at: Departamento de Física, Universidad Nacional del Sur, Av. Alem 1253, 8000 Bahía Blanca, Argentina. Tel.: +54 291 4595101x2843; fax: +54 0291 4595142.
E-mail address: egonzal@uns.edu.ar (E.A. González).

0169-4332/$ – see front matter © 2013 Elsevier B.V. All rights reserved.
http://dx.doi.org/10.1016/j.apsusc.2013.11.023

production costs via increased Pt utilization and decreased Pt loading [15].

Platinum and other noble metal have long been added as promoters in the catalyzed Fischer–Tropsch process (CO hydrogenation) used in the conversion of gases to liquid fuels [16–23]. In the case of CO reduction, the Pt promoter acts to enhance overall Fischer–Tropsch activity by increasing the reducibility of cobalt oxides, thus increasing the availability of active metal sites and concentration of intermediates adsorbed on the catalyst [20–22]. The exploration of CO_2 as well as CO in Fischer–Tropsch type chemistry is a promising strategy for the production of oxygenated hydrocarbons and increasingly desirable goal because of their use in fuels and as chemical feedstocks [24].

Cobalt is well known for its use in the catalytic hydrogenation reactions of CO and CO_2 to produce gaseous or liquid hydrocarbons, with a long history of producing synthetic fuels. A significant number of previous studies have been conducted on CO oxidation of Co oxide or Co–Pt bimetallics [25–31]. In these studies it has been suggested that the oxidation state of Co plays a critical role in the catalytic reaction mechanism: specifically, cobalt oxide provides oxygen to combine with the adsorbed CO molecules and Co is itself then re-oxidized to provide a new active site. Zheng et al. [32] consider its role in the model oxidation reaction of CO to CO_2 on CoPt nanoparticles. The goal of that work is understand the role of oxidation state and elemental composition changes of one such typical bimetallic catalyst's surface reactivity through a combined catalytic and in situ spectroscopic study of bimetallic CoPt nanoparticles used as catalysts for CO [32].

The Pt—Co alloy system has been used for multiple purposes, because of its interesting magnetic and catalytic behavior [33–37]. Pt—Co has been found to be an active catalyst in the Fischer–Tropsch process and low-temperature oxidation and reduction reactions, respectively [4,12]. It is a well-known fact and the basis of many of today's technological applications that the catalytic properties of alloys are often superior to those of pure metals [38].

Gauthier et al. [39] reported an STM study of CO adsorption on a PtCo(1 1 1) surface. Comparing images with chemical contrast of the alloy constituents and images of the same surface area showing the CO molecules, these authors determined the adsorption sites of CO and to directly demonstrate the ligand effect for CO adsorption on this surface. They found that the CO molecule, at low coverage, reside on top of Pt atoms with at least one Co neighbor atom in the surface; moreover, the Co ligands influenced on the strength of Pt—CO bond.

Fenske et al. [40] also observed ligand effect when adsorbed CO on Co—Pt alloy surfaces through Fourier transform infrared reflection absorption spectroscopy (FT-IRRAS) and temperature-programmed desorption (TPD) spectroscopy. These authors found that the CO adsorption behavior depend strongly on the composition of the surface and the first subsurface atomic layer. In the case of low Co concentrations at the surface CO adsorbs preferentially on Pt sites (with an enthalpy of adsorption which is substantially lowered when compared to CO adsorption on Pt single crystals, TPD shifts of ~60 K); however, when Co dominates the surface composition, CO adsorbs preferentially on Co sites (with enthalpy of adsorption leading to a TPD shift by ~80 K to higher temperatures with respect to monometallic single crystals). This behavior can be explained by an electronic influence of the presence of a second metal in the chemical environment of a given adsorption center [40].

In this work we modeled the benzene and CO co-adsorption on a PtCo alloy studying the changes in the electronic structure and chemical bonding after adsorption.

2. The surface model and the computational method

The crystal structure of the PtCo alloy presents two-phases. A chemically disordered face centered cubic (FCC) phase, which correspond to low temperature structure, and a chemically ordered $L1_0$ or face-centered tetragonal (FCT) structure for high temperature. In this work we have modeled the last one with a space group P4/mmm. The reason for that choice is that under operation condition in fuels electrodes the high temperature phase is the most stable. Stassi et al. [41] studied the thermal effect on the two stable structure for PtCo alloys and found that both catalysts showed good performance under PEMFC operation; however, the catalyst characterized by the disordered FCC structure performed slightly better at low temperature (80 °C) and full humidification; whereas, the primitive cubic ordered structure catalyst showed superior characteristics both in terms of performance and stability at high temperature (110 °C) and low relative humidity. These last operating conditions are more relevant for automotive applications.

The calculated a and c lattice parameters for PtCo FCT bulk are 3.81 and 3.71 Å, respectively. They are in good agreement with the experimental data, which are 3.78 and 3.71 Å [42], respectively, and also agrees with the values obtained by Hirunsit and Balbuena [43] and other literature values (3.812 and 3.708 Å) [44]. We selected the (1 1 1) crystallographic plane to study the benzene and CO co-adsorption because we found it as the most stable surface, in coincidence with previous calculation of Hirunsit and Balbuena [43] and Dannenberg et al. [45]. Density functional theory (DFT) is used to compute adsorption energies, trace relevant orbital interactions and to discuss the electronic consequences of incorporating C_6H_6 first and CO later to the surface. In the next sections, we will consider the computational method and the adsorption models.

2.1. Computational method

We performed first principles calculations based on spin polarized DFT. The Vienna Ab-initio Simulation Package (VASP) is used to solve the Kohn–Sham equations with periodic boundary conditions and a plane wave basis set [46–48]. The electron–ion interactions were described by ultra-soft pseudopotentials [49], and the exchange and correlation energies were calculated with the Perdew–Burke–Ernzerhof form of the spin-polarized generalized gradient approximation (GGA-PBE) [50]. We used a kinetic energy cutoff of 300 eV for all calculations, which converges the total energy to ~1 meV/atom and 10^{-4} Å for the primitive cell of bulk. The Monkhorst–Pack scheme was used for the k-point sampling [51]. Equilibrium lattice constants of 3.81 and 3.71 Å are used with a converged mesh of $7 \times 7 \times 7$. Bader analysis was used to calculate electronic charges of atoms before and after adsorption [52].

We defined the stabilization energy PtCo—C_6H_6—CO with respect to isolated atoms as:

$$\Delta E_{ads} = E_{ads}\left(\frac{(C_6H_6 + CO)}{PtCo}\right) - E_{Total}(PtCo) - E_{Total}((C_6H_6)_{molec}) - E_{Total}(CO_{molec})$$

where $E_{Total}((C_6H_6)_{molec})$ and $E_{Total}(CO_{molec})$ are the energy of the isolated benzene and CO molecules.

To understand the $(C_6H_6 + CO)$/PtCo interactions and bonding we used the concept of density of state (DOS) and the crystal orbital overlap population (COOP) as described by Hoffmann [53]. The COOP curve is a plot of the OP weighted DOS vs energy. Looking at the COOP, we analyze the extent to which specific states contribute to a bond between atoms or orbitals [53]. The Overlap Populations and COOP analysis were performed using the Spanish Initiative

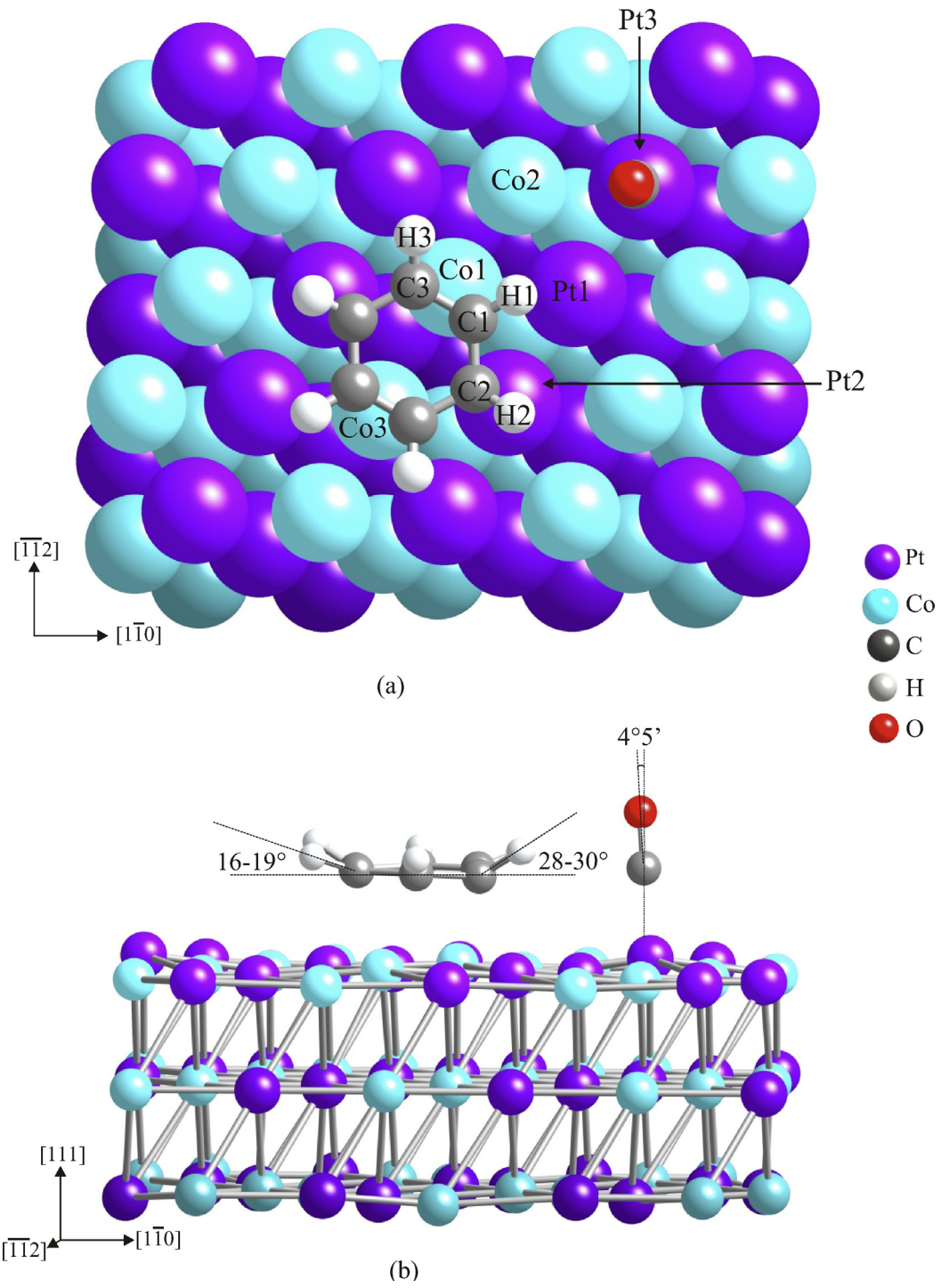

Fig. 1. (a) Schematic top view of the $((C_6H_6)_{BRIDGE} + CO)$ on PtCo(1 1 1) surface. The grading color indicates the inner layers. (b) Schematic lateral view where the C—H and C—O angles are indicates. Pt Co C H O..

for Electronic Simulations with Thousands of Atoms (SIESTA) code [54,55]. We adopted the generalized gradient approximation (GGA) to treat the electronic exchange and correlation effects, as described by Perdew–Burke–Ernzerhof [56]. In all procedures, a split-valence double-ζ basis set of localized numerical atomic orbitals was used, including polarization functions (DZP), with an energy shift of 50 meV and a split norm of 0.15 [55,57]. An energy cutoff of 250 Ry for the grid integration was chosen to represent the charge density [54]. The basis set superposition error (BSSE) was eliminated by adding ghost atoms to the calculation on the isolated adsorbate. Ghost atoms possess basis functions as normal but do not otherwise affect the calculation (no projectors, compensation charges, and so on), thereby ensuring that the same degrees of freedom are available to the wave functions in any calculation. This procedure is called the counterpoise method and is described in detail in Ref. [58]. Standard norm-conserving Troullier–Martins pseudopotentials [59] in their fully separable form [60] were used to describe the electron–ion interaction. The following electronic states were

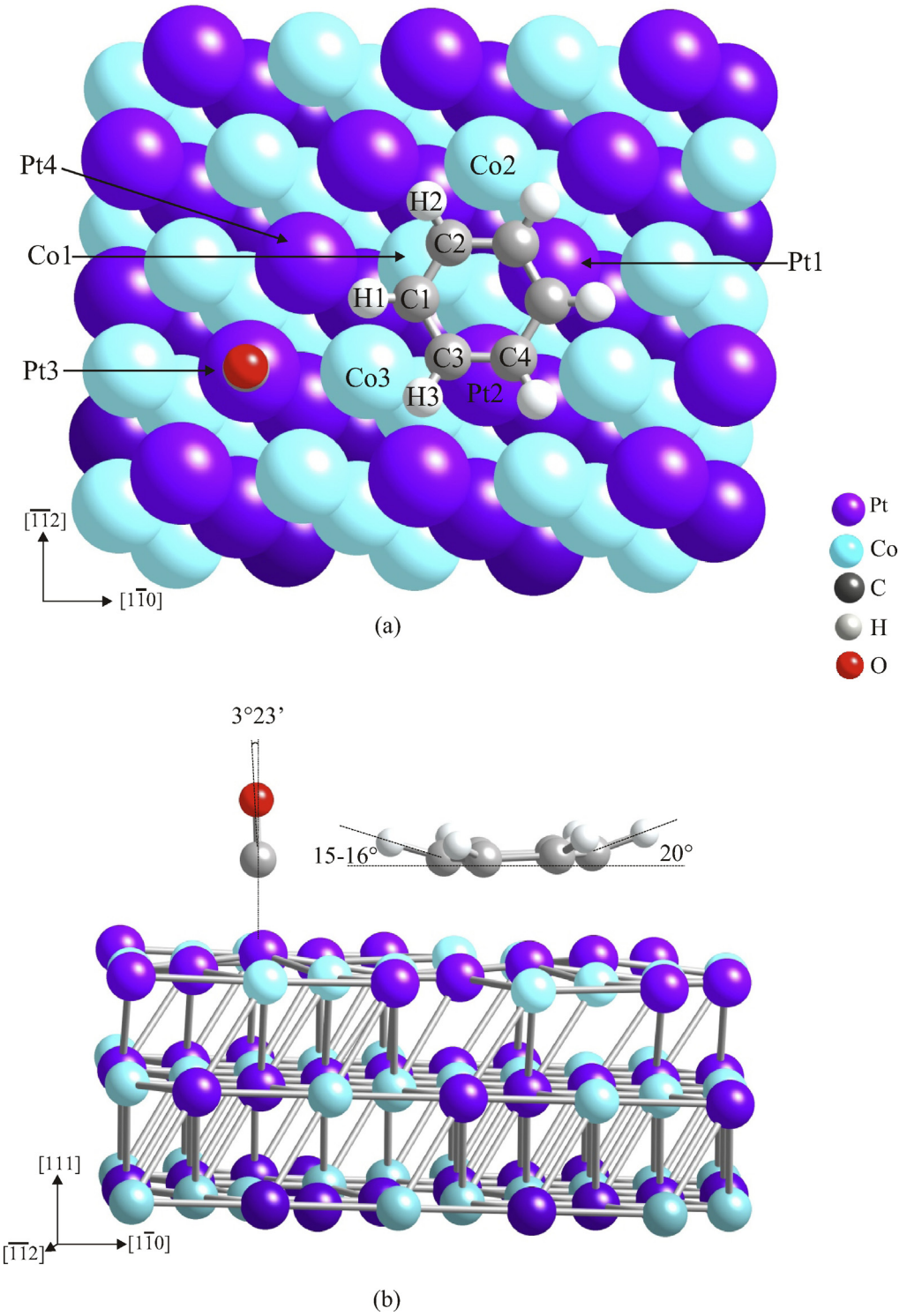

Fig. 2. (a) Schematic top view of the $((C_6H_6)_{HCP} + CO)$ on PtCo(1 1 1) surface. The grading color indicates the inner layers. (b) Schematic lateral view where the C—H and C—O angles are indicates. Pt Co C H O..

considered as valence in the pseudopotential description of the atoms: Pt $5d^9\ 6s^1$; Co $3d^7\ 4s^2$; C $2s^2\ 2p^2$; H 1s and O $2s^2\ 2p^3$.

2.2. The (1 1 1) surface and adsorption models

In a previous work we studied the benzene adsorption on PtCo and calculated the stability of the ordered atomic planes (0 0 1), (1 0 0), and (1 1 1) in FCT PtCo structure. The most stable plane of PtCo FCT result to be the (1 1 1) [61], in coincidence with calculations of Hirunsit and Balbuena [43] and Dannenberg et al. [45]. Note that the results of that study do not address the alloy surface stability, which can be determined using surface free energy and surface segregation energy as recently reported [62].

Table 1
Electron orbital occupation, overlap population, charge and distances for PtCo(1 1 1) clean, C_6H_6 and CO (vacuum).

Structure	Electronic occupation			Bond type	OP	Distances (Å)
	s	p	d			
PtCo(1 1 1)						
Pt	1.06	1.94	8.80	Pt–Pt	0.663	2.650
Co	0.47	0.20	6.09	Co–Co	0.128	2.664
				Pt–Co	0.237	2.673
C_6H_6						
C	0.93	1.46	0.00	C–C	0.740	1.398
H	0.89	0.00	0.00	H–H	0.000	2.490
				C–H	0.754	1.092
CO						
C	0.44	0.38	0.00	C–O	0.854	1.143
O	1.61	3.56	0.00			

We represented the (1 1 1) plane with a supercell. In order to achieve the best compromise between computational time and accuracy of our model, we decided to use a seven layers slab separated in the [1 1 1]-direction by vacuum regions. The thickness of the vacuum region, corresponding to 6 layers (>13 Å), was enough to avoid interaction of the benzene molecules on the surfaces. The thickness of PtCo(1 1 1) slab should be such that it approaches the electronic structure of 3D bulk PtCo in its innermost layer. Our slab has two surface-like layers and four inner layers. For the sake of clarity, Figs. 1 and 2 only show the first three layers of the slab.

For benzene adsorption on the PtCo(1 1 1) surface at low coverage, the molecule-surface distance was optimized considering relaxation for the first four layers of the metal slab until 1 meV convergence is obtained in the total energy; the three remaining layers (bulk like) were maintained (kept) fixed. In our previous work, we mapped the molecular adsorption in all the high symmetry sites of the (1 1 1) surface and we found that the most stable sites for benzene adsorption is bridge and an HCP sites, but with different molecular orientation [61]. In the bridge site the benzene molecule is located rotated 30° respect to the orientation in the HCP site (see Figs. 1 and 2).

The adsorption of the CO on PtCo(1 1 1) has been already experimentally studied. Gauthier et al. [39] found that this molecule adsorbs on top of a Pt atom at low coverage. Thus, to start our co-adsorption model, we located the CO molecule on top of a Pt atom nearby the aromatic ring and let the system to relax. Two possible neighboring Pt atoms have been considered to be the top adsorption site location, one close the carbon ring but without touch (Pt3 in Figs. 1 and 2) and other almost touching the ring. The final geometries are shown in Figs. 1 and 2.

Table 2
Electron orbital occupation, overlap population, ΔOP%, Δcharge and distances for $(C_6H_6)_{BRI\ 2B}$ + CO/PtCo(1 1 1).

Structure	Electronic occupation			ΔCharge	Bond type[a]	OP	ΔOP%[b]	Distances (Å)
	s	p	d					
Pt1	1.01	1.76	8.74	0.712	Pt1–Pt2	0.589	−11.2	2.670
Co1	0.33	0.17	6.01	0.233	Co1–Co2	0.198	+54.7	2.520
					Co1–Co3	0.039	−69.5	3.001
					Pt1–Co1	0.309	+30.4	2.548
					Pt2–Co3	0.197	−16.9	2.681
C1	0.96	3.10	0.00	−1.973	C1–C2	0.921	+24.4	1.470
					C1–C3	1.114	+50.5	1.418
H1	1.02	0.00	0.00	−0.250	C1–H1	0.892	+18.3	1.098
					Pt2–C2	0.503	–	2.181
					Pt1–H1	0.002	–	2.839
					Co1–C1	0.173	–	2.124
C_{CO}	1.03	2.51	0.00	−2.805	C_{CO}–O	0.741	−13.2	1.161
O	1.60	5.12	0.00	−2.143	C_{CO}–Pt3	1.455	–	1.866
Pt3	0.89	1.96	7.98	1.285	C_{CO}–Co2	0.008	–	3.307
					C_{CO}–H1	0.0001	–	3.425

[a] The geometry of the OP is shown in Fig. 1.
[b] The percentage of chance is respect to the clean surface or the molecules in vacuum.

Table 3
Electron orbital occupation, overlap population, ΔOP%, charge and distances for $(C_6H_6)_{HCP1A}$ + CO/PtCo(1 1 1).

Structure	Electronic occupation			ΔCharge	Bond type[a]	OP	ΔOP%[b]	Distances (Å)
	s	p	d					
Pt1	0.85	1.63	8.31	0.989	Pt1–Pt2	0.484	−27.0	2.710
Co1	0.33	0.18	5.96	0.376	Co1–Co2	0.100	−21.9	2.691
					Co1–Co3	0.124	−3.1	2.645
					Pt1–Co1	0.188	−20.7	2.731
					Pt2–Co3	0.248	+4.6	2.617
C1	0.96	3.13	0.00	−1.704	C1–C2	1.056	+42.7	1.458
					C1–C3	0.984	+33.0	1.426
H1	1.03	0.00	0.00	−0.134	C1–H1	0.892	+18.3	1.097
					C4–Pt2	0.348	–	2.226
					C2–Co1	0.175	–	2.115
					H1–Pt4	0.007	–	2.820
C_{CO}	1.04	2.50	0.00	−2.801	C_{CO}–O	0.738	−13.6	1.165
O	1.60	5.12	0.00	−2.148	C_{CO}–Pt3	1.460	–	1.863
Pt3	0.89	1.93	7.96	1.329	C_{CO}–Co3	0.006	–	3.309
					C_{CO}–H1	0.001	–	3.090

[a] The geometry of the OP is shown in Fig. 2.
[b] The percentage of chance is respect to the clean surface or the molecules in vacuum.

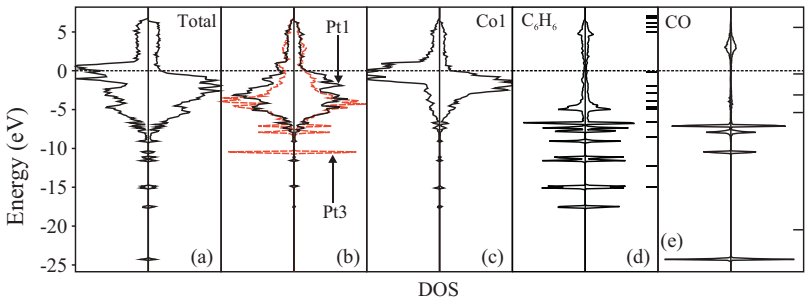

Fig. 3. DOS curves for the $((C_6H_6)_{BRIDGE} + CO)/PtCo(1\,1\,1)$. (a) Total, (b) projected on Pt atom from surface (fill line) and on Pt atom below CO molecule (dashed red line), (c) projected on Co atom, (d) projected DOS curves for the benzene molecule after the co-adsorption and (e) projected DOS curves for CO molecule after the co-adsorption. The bars in the right side indicate the molecular level in vacuum. (For interpretation of the references to color in this figure legend, the reader is referred to the web version of the article.)

3. Results and discussion

As mentioned before, we have previously reported the benzene adsorption on PtCo(1 1 1) [61]. The most stable sites are a bridge Co—Co (BRI 2) and a hollow builds by 2 Pt and 1 Co atoms (HCP 1). In order to study the co-adsorption, the CO molecule was located on a Pt-top site neighbor to the benzene molecule. After optimization we found that the carbon monoxide molecule remain on top of Pt atom but shift from the center of the metal atom forming an azimuthal angle respect of this atom and a tilted geometry. In the case of the benzene in the bridge site, from the two possible Pt top location only one site result to be favorable, where the azimuthal angle is about 46°4′ and the tilt angle is 4°5′. In the case of the HCP site, the two locations for top site are favorable. In the more favorable geometry, the azimuthal and tilt angles are about 52°21′ and 3°23′, respectively; meanwhile, in the less favorable case (+0.34 eV respect to the former one reported), the angles are about 22°27′ and 13°23′, respectively. Because of the results do not have significatively changes only the more favorable situation is report in the HCP case. The final geometry is shown in Figs. 1 and 2 (for sake of simplicity only the tilt angles are indicated). The preference of CO adsorption on Pt agrees with previous experiments. The adsorption energies previously determined for low doses of CO on Pt(1 1 1) [63] are somewhat higher than those on the close-packed Co surface [64]. The difference in adsorption energies E_{ads} obviously does not change its sign in the alloy. Stronger CO adsorption on Pt than on Co may seem counterintuitive, as it does not follow the trend of decreasing reactivity with increasing filling of the d shell. It is known, however, that magnetism of the 3D elements can weaken adsorption significantly and thus counteract this trend [39].

The benzene and CO co-adsorption is a favorable process on PtCo(1 1 1). For benzene adsorbed in the bridge site the adsorption/stabilization energy is −1.60 eV, whereas for the HCP site is −1.62 eV. The optimized geometries from DFT calculation are shown in Figs. 1 and 2. We can compare the co-adsorption energies with the CO and benzene alone adsorption. Considering CO adsorption in the same condition – like in the co-adsorbed system – the lowest energy is −1.08 eV atop on a Pt atom. In the case of benzene alone the energies are −0.32 eV and −0.28 eV in the bridge and HCP site, respectively [61]. If we add CO and benzene alone energies, the total energy of the system would be −1.40 eV (benzene bridge) and −1.36 eV (benzene HCP). These values are both less stables than the co-adsorbed cases.

We found that the ring geometry was slightly distorted in all the possible adsorption sites [61]. The carbon atoms lie about ∼2.1 Å above the first surface layer. The carbon ring was slightly expanded after adsorption —C—C increase from 1.398 Å in vacuum to 1.475 and 1.457 Å in BRI2 and HCP1 sites, respectively. In both sites, the metal atoms directly below the aromatic molecule move upward toward the C-ring [61]. When the co-adsorption is considered, the $C_{C_6H_6}$—$C_{C_6H_6}$ distances are shortened in both sites (1.418 Å for BRI2 and 1.426 Å for HCP1 site) (see Tables 1 and 2). Also, the Pt atom under the CO molecule moves upward. As mentioned before, the CO molecule present a tilt angle after adsorption of 4°5′ for the bridge site and of 3°23′ in the case of the HCP site (see Figs. 1b and 2b). To the best of our knowledge, no tilt angle for the CO adsorbed in Pt(1 1 1) or PtCo(1 1 1) has been previously reported. The computed H-tilt angles for the benzene do not present significant changes after the co-adsorption.

The shortest $C_{C_6H_6}$—Co bond is 2.124 Å for BRI2 and 2.115 Å for HCP1 (see Tables 1 and 2). This values are slightly smaller than that reported of the benzene adsorption alone on PtCo(1 1 1) (2.145 Å for BRI2 and 2.132 Å for HCP1) [61]. In the case $C_{C_6H_6}$—Pt, the computed values are 2.181 (HCP1) and 2.184 Å (BRI2) (see Tables 1 and 2), which are similar to those previously obtained (2.237 and 2.173 Å, respectively) [61].

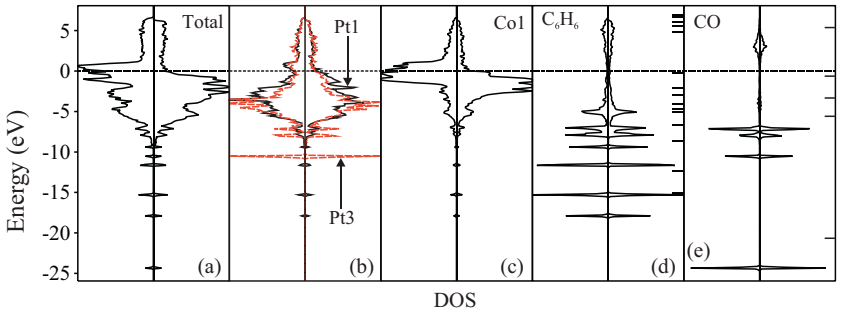

Fig. 4. DOS curves for the $((C_6H_6)_{HCP} + CO)/PtCo(1\,1\,1)$. (a) Total, (b) projected on Pt atom from surface (fill line) and on Pt atom below CO molecule (dashed red line), (c) projected on Co atom, (d) projected DOS curves for the benzene molecule after the co-adsorption and (e) projected DOS curves for CO molecule after the co-adsorption. The bars in the right side indicate the molecular level in vacuum. (For interpretation of the references to color in this figure legend, the reader is referred to the web version of the article.)

The computed Pt and Co electron orbital populations for the clean surface are $6s^{1.06}\,6p^{1.94}\,5d^{8.80}$ and $4s^{0.47}\,4p^{0.20}\,3d^{6.07}$ respectively. After co-adsorption, the computed electron orbital populations are Pt $6s^{1.01}\,6p^{1.75}\,5d^{8.72}$ and Co $4s^{0.33}\,4p^{0.17}\,3d^{6.01}$ for the benzene adsorbed in the bridge site and Pt $6s^{0.85}\,6p^{1.63}\,5d^{8.31}$ and Co $4s^{0.33}\,4p^{0.18}\,3d^{5.96}$ for the benzene adsorbed in the HCP site. A charge transfer is computed from Co toward Pt as expected from the electronegativity difference.

Considering the CO adsorption on a metal surface, the metal-C_{CO} and the C_{CO}—O bond strengths strongly depend on the donation (from the bonding orbitals of the CO to the antibonding of the metal) and back-donation (from the bonding orbitals of the metal to the antibonding orbitals of the CO), respectively. The 4 and 5σ orbitals of CO donate electrons to the metal and, by back-donation, the π^* orbitals which are C_{CO}—O antibonding receive electrons. In both considered situations, the Pt—C_{CO} distance is similar (~1.86 Å) as well as the OP bond (~1.46), being this OP bond the most important (see Tables 2 and 3). The C_{CO}—O OP bond after the co-adsorption is reduced about 13% in both situations. The Pt atom below the carbon monoxide molecule is more affected than the rest of the surface atoms and a decrease in the d orbital population is observed for this metal atom (from $5d^{8.80}$ to $5d^{8.72}$ and $5d^{7.79}$) (see Tables 2 and 3).

The electronic structure (DOS plots) of the surface slab and the adsorbed molecules are shown in Figs. 3 and 4. The total DOS shows a similar behavior after the co-adsorption in both considered situations (see Figs. 3a and 4a). The series of small peaks between −10.5 and −18.1 eV in Figs. 3a–d and 4a–d coming from the benzene molecular orbitals stabilized after the adsorption (see the bars on the right in Figs. 3d and 4d). A higher hybridization in the region (−6.5, −9.2) eV is present for both benzene adsorption sites showing an interaction of the benzene orbitals with the bottom of the d metal band (see Figs. 3b and c and 4b and c). The peaks at −24.2 and −10.4 eV correspond to the CO-surface interaction (see Figs. 3a and 4a). The CO—Pt strongest interaction can be observed in the Pt3 (dashes red line) projected DOS (see the peaks at −10.2, −8.1 and −6.4 eV comparing Figs. 3b and 4b dashed red line with Figs. 3e and 4e).

Both benzene and CO states on PtCo(1 1 1) show high hybridization. The benzene molecules shows more important peak that when it is adsorbed alone especially in the region (−17.5, −6.2) eV. In that region, CO also shows important peaks where the more important correspond in energy with benzene. This could indicate a molecule–molecule interaction, especially between −7.5 and −6.2 eV (see Figs. 3d and e and 4d and e).

Regarding the bonding, in both studies situation almost all metal–metal OP decrease being the most affected the atom bonding below the benzene molecule (see Tables 2 and 3). The Pt—Pt COOP curves are similar in both considered cases (compare Figs. 5 and 6). The Co—Co bond distances are influenced by the adsorption of benzene. In the case of the BRI site, the two Co atoms that form the adsorption site (Co1 and Co3) are moved upward leading to a decrease in this OP, whereas the Co1—Co2 OP is increased and the distance is shortened (see Table 2 and Fig. 5b). In the HCP case, the Co atoms below the aromatic ring moved away and these OP are weakened (see Table 3 and Fig. 6b). The Pt1—Co1 OP increases because the distance between these atoms becomes shorter after the benzene adsorption in the bridge situation (2.548 Å vs 2.673 Å in the clean surface) meanwhile in the HCP site is elongated (stretched) (2.731 Å vs 2.673 Å) (see Tables 1–3 and Figs. 5c and 6c).

The benzene OP bonds are increased after adsorption. The $C_{C_6H_6}$—$C_{C_6H_6}$ OP in both sites increase due to bonding interaction with the d metal bond (see bonds between −6.9 and −1.5 eV) (compare Figs. 7a and 8a with 7c and 8c). Similar behavior is detected for $C_{C_6H_6}$—H bonds (compared Figs. 7b and 8b with 7d and 8d).

The Pt—C and Co—C bonds are developed with benzene and carbon monoxide. The Pt—C OP more important OP is obtained between the carbon atom of the CO molecule and the Pt atom below. The Pt—C_{CO} distance is similar in both situations (1.455 Å for BRI and 1.460 Å for HCP site) (see Tables 2 and 3 and compare Figs. 9 and 10).

The carbon monoxide OP bond is weakened about 13% after adsorption in both cases (see Tables 2 and 3) (see Figs. 9c and 10d). Also, small Pt—H, Co—C_{CO} and H—C_{CO} OP are found in both cases (see Tables 2 and 3 and Figs. 7d and 8d, 9b and 10b, and 9d and 10d). In our previous work, no Pt—H bond was detected [63]. The small H—C_{CO} OP could indicate a very small benzene–CO interaction that is not found in the co-adsorption on pure Pt(1 1 1) [65] but it is does on Co(0 0 0 1) [66].

Finally, we also computed the vibrational frequencies for the chemisorbed molecules. As a reference, the vibrational frequencies of gas-phase benzene were calculated for the A_{1g} and B_{2u} modes in a previous work [61]. The vibrational frequencies calculated for the adsorbed molecules are listed in Table 4. The frequencies from the co-adsorbed benzene molecule are similar from those adsorbed

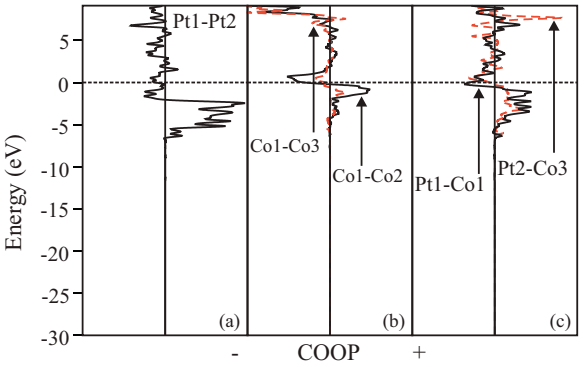

Fig. 5. COOP curves for $((C_6H_6)_{BRIDGE} + CO)$/PtCo(1 1 1). (a) Pt—Pt, (b) Pt—Co and (c) Co—Co bonds.

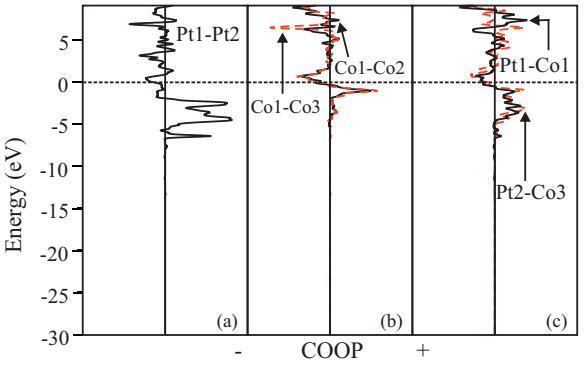

Fig. 6. COOP curves for $((C_6H_6)_{HCP} + CO)$/PtCo(1 1 1). (a) Pt—Pt, (b) Pt—Co and (c) Co—Co bonds.

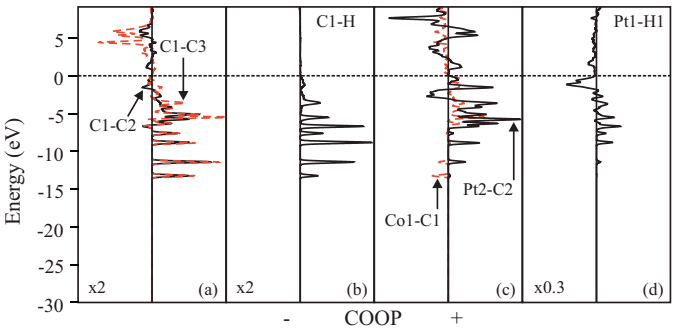

Fig. 7. COOP curves for $((C_6H_6)_{BRIDGE} + CO)$/PtCo(1 1 1). (a) $C_{C_6H_6}$—$C_{C_6H_6}$, (b) $C_{C_6H_6}$—H, (c) Pt—$C_{C_6H_6}$ and Co—$C_{C_6H_6}$ and (d) Pt–H bonds.

Table 4
Frequencies of the A_{1g} and B_{2u} modes of benzene and CO (TOP site) adsorbed (in cm^{-1}).

	Pt(1 1 1)[a]		Pt(1 1 1)[b]	Pt(1 1 1)[c]	Pt(1 1 1)[d]	Previous work		This work	
	BRI 30°	HCP 0°	HREELS	EELS	B3PW91	BRI 2B	HCP 1A	BRI 2B	HCP 1A
A_{1g}	826	860	825	–	–	835	870	850	888
A_{1g}	3103	3125	3015	–	–	3022	3050	3018	3035
B_{2u}	1140	1154	1130	–	–	1136	1139	1136	1136
B_{2u}	1313	1345	1305	–	–	1321	1333	1343	1356
C–O	–	–	–	2100	2139	–	–	1967	1948
Pt–C	–	–	–	470	495	–	–	489	490

[a] Taken from Ref. [14].
[b] Taken from Ref. [67].
[c] Taken from Ref. [68].
[d] Taken from Ref. [69].

alone respectively in pure FCC Pt(1 1 1) [14,67–69] and PtCo(1 1 1) [61]. The lowering in the vibration frequencies modes involving C—C bonds is consistent with the stretching of these bonds (see Tables 1–3) and Pt, Co—C bond formation. Lehwald et al. [70] have explained the shifts in HREELS vibration frequencies of benzene on Pt (1 1 1) and Ni(1 1 1) by electronic interaction between the metal d-orbitals and molecules adsorbed in on top and threefold hollow sites respectively. The C—Pt and C—O frequencies for CO/PtCo(1 1 1) are in very good agreement with those obtained experimentally and by DFT calculations in pure FCC Pt(1 1 1) [68,69].

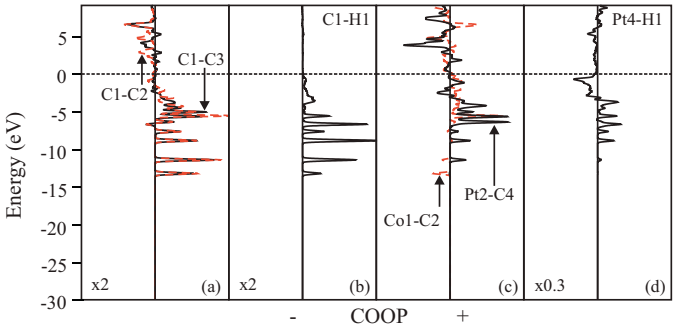

Fig. 8. COOP curves for $((C_6H_6)_{HCP} + CO)/PtCo(1\,1\,1)$. (a) $C_{C_6H_6}$—$C_{C_6H_6}$, (b) $C_{C_6H_6}$—H, (c) Pt—$C_{C_6H_6}$ and Co—$C_{C_6H_6}$ and (d) Pt–H bonds.

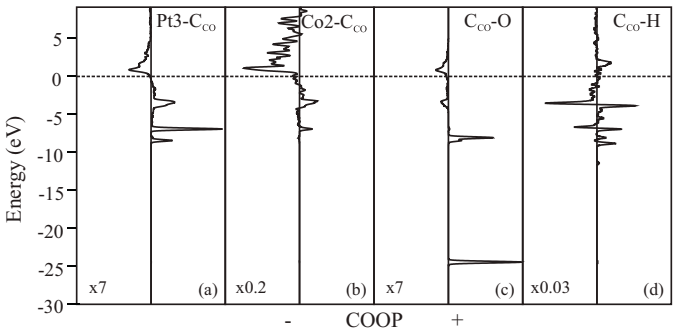

Fig. 9. COOP curves for $((C_6H_6)_{BRIDGE} + CO)/PtCo(1\,1\,1)$. (a) Pt—$C_{CO}$, (b) Co—$C_{CO}$, (c) C_{CO}—O and (d) C_{CO}—H bonds.

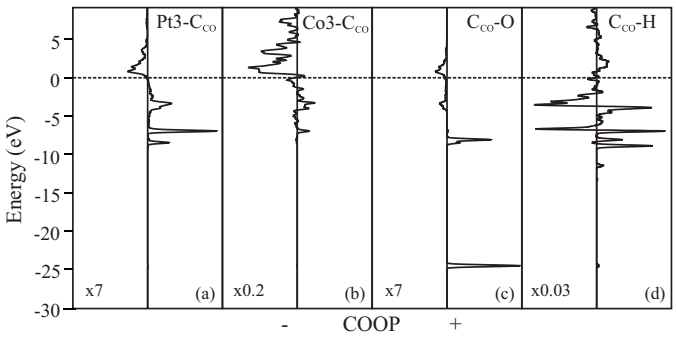

Fig. 10. COOP curves for $((C_6H_6)_{HCP} + CO)/PtCo(1\,1\,1)$. (a) Pt—$C_{CO}$, (b) Co—$C_{CO}$, (c) C_{CO}—O and (d) C_{CO}—H bonds.

4. Conclusions

We investigated the benzene and CO co-adsorption on PtCo(1 1 1) surface with an uniform distribution of metallic atoms. The most favorable system is obtained with the benzene molecule adsorbed in the HCP site formed by 2 Pt and 1 Co atoms and the CO molecule on top of a nearby Pt atom. The minimum adsorption energy is −1.62 eV. The other considered site for benzene, the bridge site, has similar adsorption energy (−1.60 eV). A large buckling is computed for both Pt and Co surface atoms. A C_{CO}—O tilt angle for CO molecule is detected being very similar in both considered cases (4°5′ and 3°23′). A higher hybridization is found showing the interaction of benzene orbitals with the bottom of the d metal band. The more developed OP is Pt—C_{CO}. A very small H—C_{CO} interaction is detected. The calculated vibrational frequencies for adsorbed benzene are similar to those reported for Pt(1 1 1) with a red-shift compared to gas-phase.

Acknowledgements

Our work was supported by ANPCyT through PICT 1770, and 320 PIP-CONICET Nos. 114-200901-00272 and 114-200901-00068 research grants, as well as by SGCyT-UNS. P.V.J., M.E.P and E.A.G. are members of CONICET. P.B. and J.S.A. are fellow researchers at this Institution. V.O. is a fellow of Comisión Investigaciones Científicas (CIC-BA).

References

[1] Y. Shao, J. Liu, Y. Wang, Y. Lin, J. Mater. Chem. 19 (2009) 46.
[2] H. Liu, C. Song, L. Zhang, J. Zhang, H. Wang, P. Wilkinson, J. Power Sources 155 (2006) 95.
[3] N. Tian, Z.Y. Zhou, S.-G. Sun, J. Phys. Chem. C 112 (2008) 19801.
[4] M. Sayes, M.-F. Reyniers, G.B. Marin, M. Neurock, J. Phys. Chem. B 106 (2002) 7489.
[5] M. Sayes, M.-F. Reyniers, M. Neurock, G.B. Marin, J. Phys. Chem. B 107 (2003) 3844.
[6] B.H. Cooper, B.B.L. Donnis, Appl. Catal. A: Gen. 137 (1996) 203.
[7] A. Stanislaus, B.H. Cooper, Catal. Rev. Sci. Eng. 36 (1994) 75.
[8] C. Morin, D. Simon, P. Sautet, J. Phys. Chem. B 108 (2004) 5653.
[9] P. Gomez-Romero, Adv. Mater. 13 (2001) 163.
[10] F.S. Tautz, Prog. Surf. Sci. 82 (2007) 479.
[11] H. Ihm, H.M. Ajo, J.M. Gottfried, P. Bera, C.T. Campbell, J. Phys. Chem. B 108 (2004) 14627.
[12] S.J. Jenkins, Proc. R. Soc. A 465 (2009) 2949.
[13] F. Mittendorfer, C. Thomazeau, P. Raybaud, H. Toulhoat, J. Phys. Chem. B 107 (2003) 12287.
[14] C. Morin, D. Simon, P. Sautet, J. Phys. Chem. B 107 (2003) 2995.

[15] A. Cheng, P. Holt-Hindle, Chem. Rev. 110 (2010) 3767.
[16] G.E. Batley, A. Ekstrom, D.A. Johnson, J. Catal. 34 (1974) 368.
[17] M.J. Dees, V. Ponec, J. Catal. 119 (1989) 376.
[18] L. Guczi, Z. Schay, G. Stefler, F. Mizukami, J. Mol. Catal. A: Chem. 141 (1999) 177.
[19] A.Y. Khodakov, J. Lynch, D. Bazin, B. Rebours, N. Zanier, B. Moisson, P. Chaumette, J. Catal. 168 (1997) 16.
[20] F. Morales, B.M. Weckhuysen, Catalysis 19 (2006) 1.
[21] D. Schanke, S. Vada, E.A. Blekkan, A.M. Hilmen, A. Hoff, A. Holmen, J. Catal. A 156 (1995) 85.
[22] S. Vada, A. Hoff, E. Ådnanes, D. Schanke, A. Holmen, Top. Catal. 2 (1995) 155.
[23] Z. Zsoldos, L. Guczi, J. Phys. Chem. 96 (1992) 9393.
[24] S. Alayoglu, S.K. Beaumont, F. Zheng, V.V. Pushkarev, H. Zheng, V. Iablokov, Z. Liu, J. Guo, N. Kruse, G.A. Somorjai, Top. Catal. 54 (2011) 778.
[25] Y.J. Mergler, A. van Aalst, J. van Delft, B.E. Nieuwenhuys, Appl. Catal. B: Environ. 10 (1996) 245.
[26] A. Torncrona, M. Skoglundh, P. Thormahlen, E. Fridell, E. Jobson, Appl. Catal. B: Environ. 14 (1997) 131.
[27] P. Thormahlen, M. Skoglundh, E. Fridell, B. Andersson, J. Catal. 188 (1999) 300.
[28] P. Broqvist, I. Panas, H. Persson, J. Catal. 210 (2002) 198.
[29] J. Jansson, A.E.C. Palmqvist, E. Fridell, M. Skoglundh, L. Osterlund, P. Thormahlen, V. Langer, J. Catal. 211 (2002) 387.
[30] M.J. Pollard, B.A. Weinstock, T.E. Bitterwolf, P.R. Griffiths, A.P. Newbery, J.B. Paine, J. Catal. 254 (2008) 218.
[31] W.L. Yim, T. Kluner, J. Phys. Chem. C 114 (2010) 7141.
[32] F. Zheng, S. Alayoglu, V.V. Pushkarev, S.K. Beaumont, C. Specht, F. Aksoyd, Z. Liud, J. Guod, G.A. Somorjai, Catal. Today 182 (2012) 54.
[33] J.L. Park, M.G. Kim, Y.W. Jun, J.S. Lee, W.R. Lee, J. Cheon, J. Am. Chem. Soc. 126 (2004) 9072.
[34] Z.T. Zhang, D.A. Blom, Z. Gai, J.R. Thompson, J. Shen, S. Dai, J. Am. Chem. Soc. 125 (2003) 7528.
[35] Y.D. Qian, W. Wen, P.A. Adcock, Z. Jiang, N. Hakim, M.S. Saha, S. Mukerjee, J. Phys. Chem. C 112 (2008) 1146.
[36] J.C. Sotelo, J.M. Seminario, J. Chem. Phys. 127 (2007) 244706.
[37] M. De Santis, R. Baudoing-Savois, P. Dolle, M.C. Saint-Lager, Phys. Rev. B 66 (2002) 085412.
[38] J.H. Sinfelt, Bimetallic Catalysts: Discoveries, Concepts, and Applications, John Wiley & Sons, New York, 1983.
[39] Y. Gauthier, M. Schmid, S. Padovani, E. Lundgren, V. Buš, G. Kresse, J. Redinger, P. Varga, Phys. Rev. Lett. 87 (2001) 036103.
[40] D. Fenske, D. Greshnykh, S. Neuendorf, D. Hoogestraat, H. Borchert, K. Al-Shamery, Surf. Sci. 602 (2008) 2101.
[41] A. Stassi, I. Gatto, G. Monforte, V. Baglio, E. Passalacqua, V. Antonucci, A.S. Aricò, J. Power Source 208 (2012) 35.
[42] L. Xiong, A. Manthiram, J. Electrochem. Soc. 152 (2005) A697.
[43] P. Hirunsit, P.B. Balbuena, Surf. Sci. 603 (2009) 912.
[44] W.B. Pearson, A Handbook of Lattice Spacings and Structures of Metals and Alloys, Pergamon, Oxford, 1964, pp. 1958–1967.
[45] A. Dannenberg, M.E. Gruner, A. Hucht, P. Entel, Phys. Rev. B 80 (2009) 245438.
[46] G. Kresse, J. Hafner, Phys. Rev. B 47 (1993) 558.
[47] G. Kresse, J. Furthmüller, Phys. Rev. B 54 (1996) 11169.
[48] G. Kresse, J. Furthmüller, Comput. Mater. Sci. 6 (1996) 15.
[49] D. Vanderbilt, Phys. Rev. B 41 (1990) 7892.
[50] J. Perdew, J.A. Chevary, S.H. Vosko, K.A. Jackson, M.R. Pederson, Phys. Rev. B 46 (1992) 6671.
[51] H.J. Monkhorst, J.D. Pack, Phys. Rev. B 13 (1976) 5188.
[52] R.F.W. Bader, Atoms in Molecules – A Quantum Theory, Oxford University Press, Oxford, 1990.
[53] R. Hoffmann, Solid & Surface: A Chemist's View of Bonding in Extended Structures, 1st ed., Wiley-VCH, New York, 1989.
[54] P. Ordejón, E. Artacho, J.M. Soler, Phys. Rev. B 53 (1996) R10441.
[55] J.M. Soler, E. Artacho, J.D. Gale, A. Garcia, J. Junquera, P. Ordejón, D. Sanchez-Portal, J. Phys. Condes. Matter 14 (2002) 2745.
[56] J.P. Perdew, K. Burke, M. Ernzerhof, Phys. Rev. Lett. 77 (1996) 3865.
[57] J. Junquera, O. Paz, D. Sanchez-Portal, E. Artacho, Phys. Rev. B 64 (2001) 235111.
[58] S.B. Boys, F. Bernardi, Mol. Phys. 19 (1970) 553.
[59] N. Troullier, J.L. Martins, Phys. Rev. B 43 (1991) 1993.
[60] L. Kleinman, D.M. Bylander, Phys. Rev. Lett. 48 (1992) 1425.
[61] P. Bechthold, S. Ardenghi, V. Cardoso Schwindt, E.A. González, P.V. Jasen, V. Orazi, M.E. Pronsato, A. Juan, Appl. Surf. Sci. 282 (2013) 17.
[62] R.K. John, R. Karsten, S. Matthias, Phys. Rev. B 77 (2008) 075437.
[63] (a) H. Froitzheim, Surf. Sci. 211–212 (1989) 837;
(b) E.G. Seebauer, A.C.F. Kong, L.D. Schmidt, Surf. Sci. 176 (1986) 134.
[64] (a) H. Papp, Surf. Sci. 129 (1983) 205;
(b) J. Lahtinen, J. Vaari, K. Kauraala, Surf. Sci. 418 (1998) 502.
[65] P.V. Jasen, G. Brizuela, Z. Padin, E.A. Gonzalez, A. Juan, Appl. Surf. Sci. 236 (2004) 394.
[66] E.A. Gonzalez, P.V. Jasen, J. Pierini, G. Brizuela, A. Juan, Surf. Rev. Lett. 5 (2009) 749.
[67] V. Demers-Carpentier, P.H. McBreen, J. Phys. Chem. C 115 (2011) 6513.
[68] H. Stininger, S. Lehwalf, H. Ibach, Surf. Sci. 123 (1982) 264.
[69] M. Tsuda, H. Kasai, Phys. Rev. B 73 (2006) 155405.
[70] S. Lehwald, H. Ibach, J.E. Demuth, Surf. Sci. 78 (1978) 577.